Supporting Information

High strong chitosan-based nanocomposites with aligned nanosheets and crosslinked networks

Xiaodong Yu[†a,b], Jihao Fan[†a,b], Shengquan Zheng[a,b], Linlin Ma[a,b], Xiaojing Liu[a,b], Yue Wu[a,b]
Chuangqi Zhao*[a] and Lei Jiang[a]

a School of Chemistry and Materials Science, University of Science and Technology of China, Hefei 230026, China.
b Suzhou Institute for Advanced Research, University of Science and Technology of China, Suzhou, Jiangsu 215123, China.
*Corresponding author e-mail: zhaochuangqi@ustc.edu.cn

This PDF file includes:

Supplementary Figs 1-17

Supplementary Tables 1-12

Other Supplementary Materials:

Supplementary Movie 1

Figures S1-S17

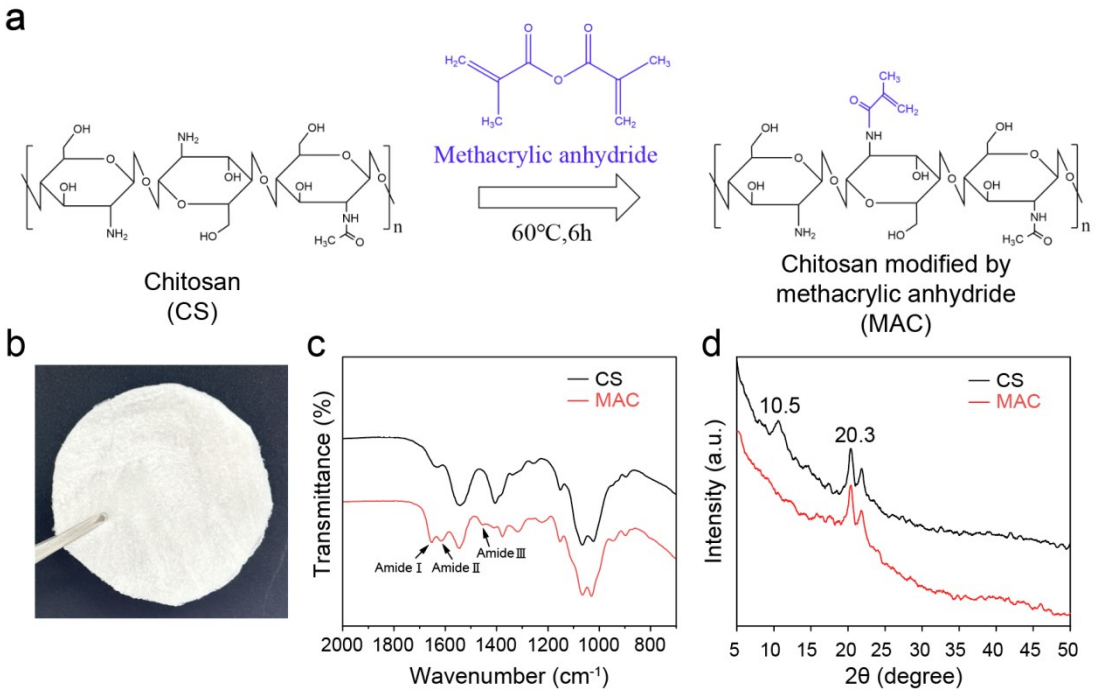

Figure S1. Synthesis and characterization of chitosan modified by methacrylic anhydride (MAC). (a) Highly chemoselective *N*-acylation reaction between chitosan (CS) and methacrylic anhydride (MA), thereby endowing MAC with photo-crosslinkable ability by introducing double bonds. (b) The MAC foam obtained after freeze-drying. (c) ATR FTIR spectra of CS and MAC. Newly formed amide absorbance was observed at 1650.1 cm^{-1}, 1616.1 cm^{-1}, 1454.1 cm^{-1}, corresponding to amide I band (C=O stretching)、amide II band (N-H deformation) and amide III band (C-N stretching) in the spectrum of MAC, respectively. (d) XRD patterns of CS and MAC. The crystalline peak at 2θ = 10.5° was disappeared in MAC, suggesting that large numbers of hydrogen bonds were destroyed along with the formation of low crystalline and/or amorphous phase.[1]

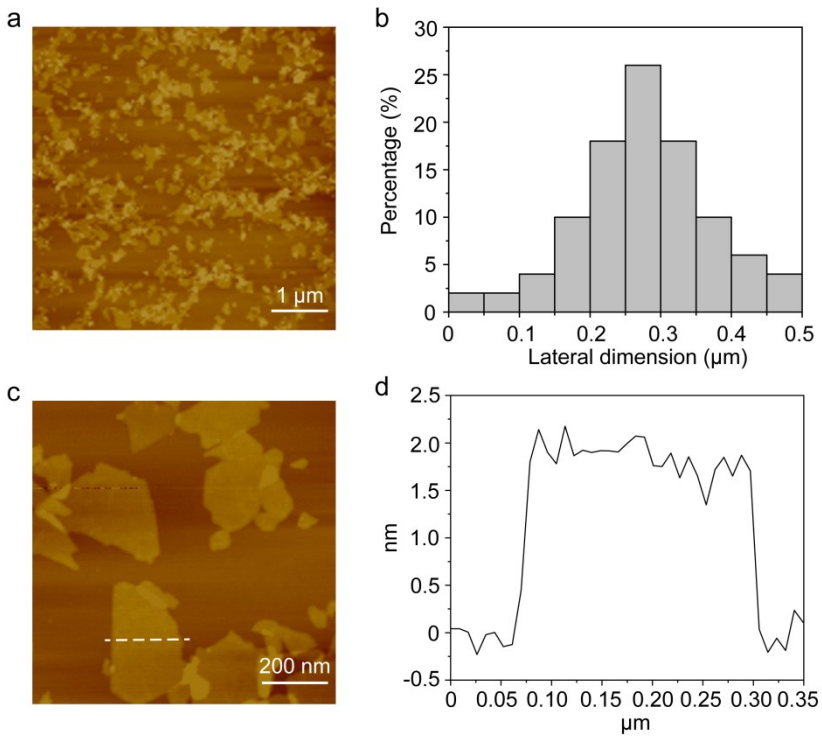

Figure S2. Characterization of the MMT nanosheets. (a) A typical AFM image of MMT nanosheets. (b) The corresponding size distribution of MMT nanosheets. (c) A typical AFM magnification image of MMT nanosheets. (d) The corresponding thickness profiles of the selected MMT nanosheet.

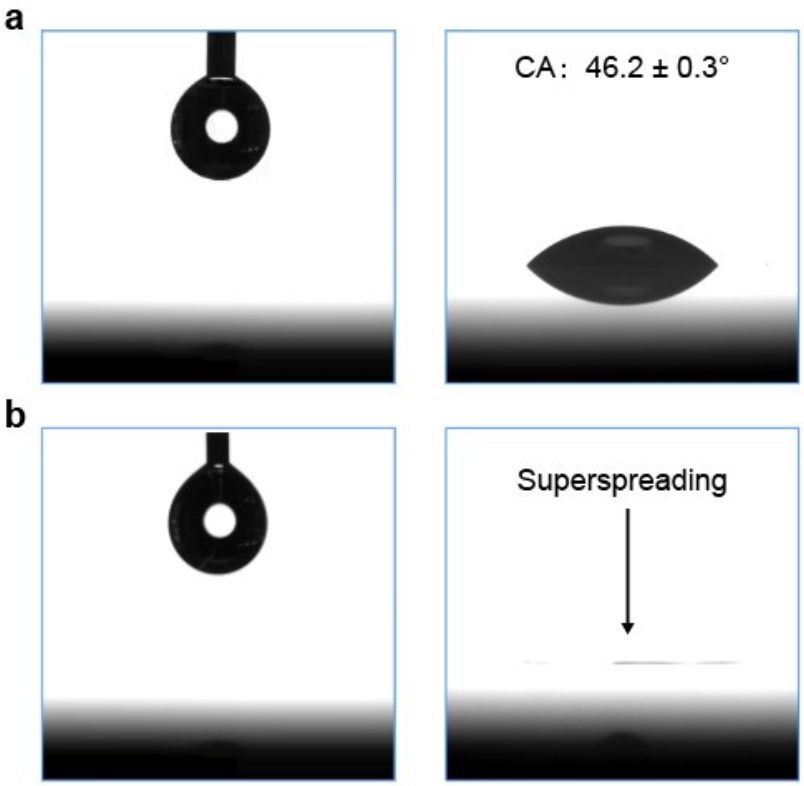

Figure S3. Water-droplet contact angle of the glass in the air (a: glass, b: Glass after vacuum plasma pretreatment). (a) The untreated glass exhibited the hydrophilic properties. (b) The liquid solution can achieve superspreading over the treated glass surface, shown in Video 1.

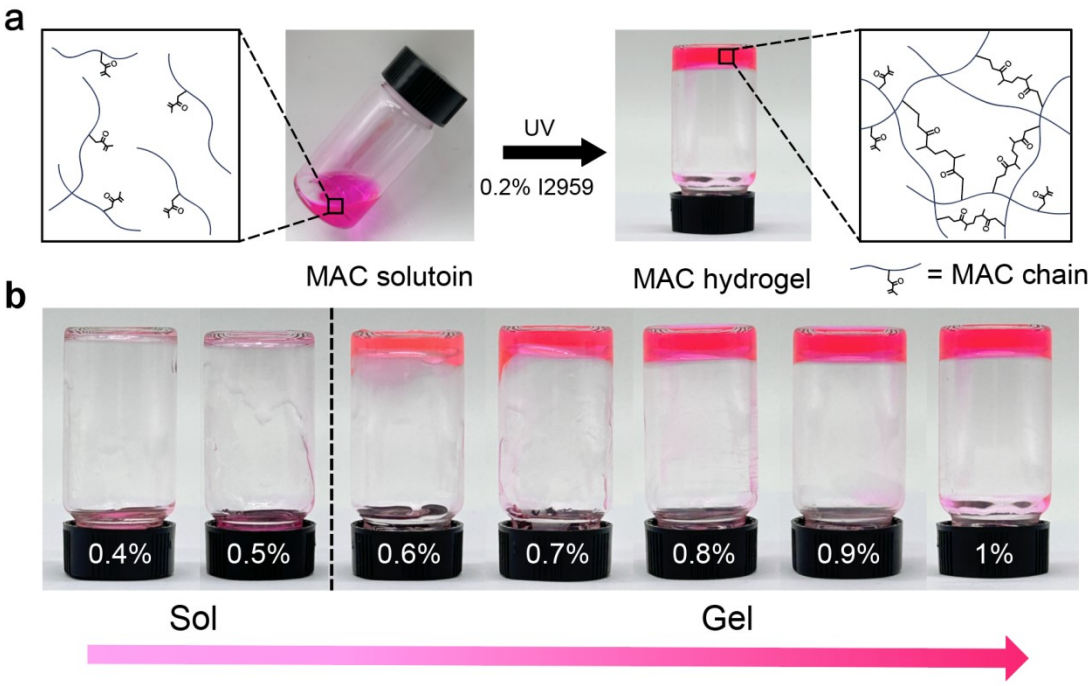

Figure S4. (a) Schematic view of the photopolymerization of MAC. (b) The influence of MAC concentration on polymerization, showing that gel cannot be obtained when MAC concentration is lower than 0.5%.

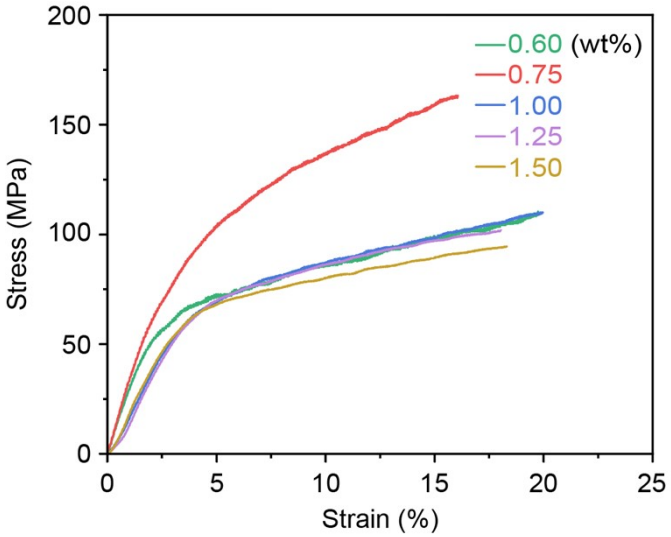

Figure S5. Tensile stress-strain curves of MAC membranes with different concentrations at 25°C and 20% relative humidity. The MAC film with a concentration of 0.75% exhibited the highest tensile strength compared to the other films. Therefore, we selected 0.75% MAC as the optimal concentration for the preparation of MAC/MMT nanocomposite films. The composition of reaction solutions and the detailed mechanical properties data are listed in Table S1.

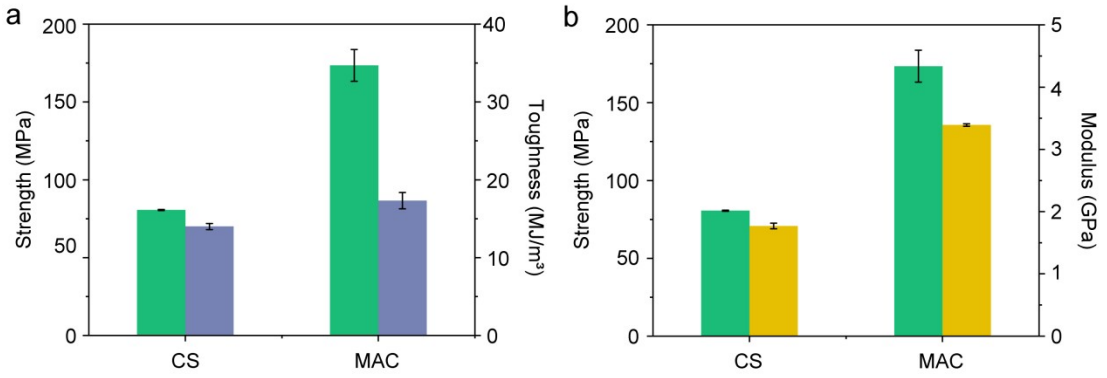

Figure S6. Mechanical properties of the CS and MAC films at 25°C and 20% relative humidity. (a) The strength and toughness. (b) The strength and modulus. The composition of reaction solutions and the detailed mechanical properties data are listed in Table S2.

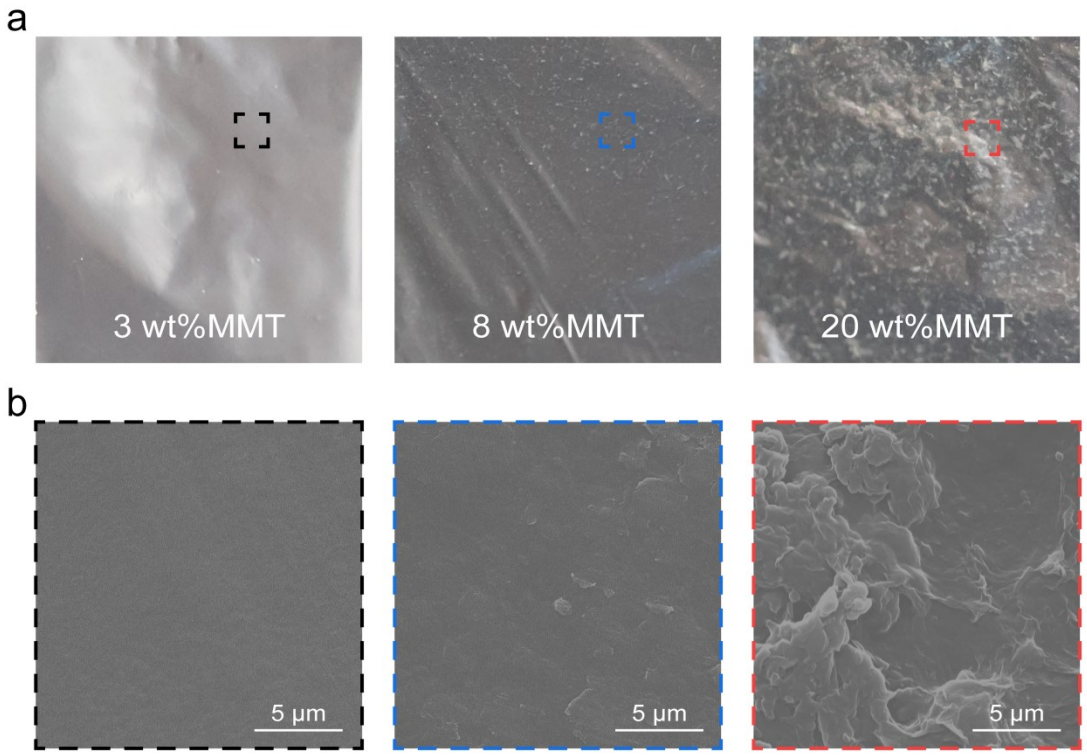

Figure S7. Macroscopic and microscopic images of MAC/MMT nanocomposite films with different MMT contents. (a) Macroscopic images of MAC/MMT nanocomposite films with different MMT contents. (b) Microscopic SEM electron microscope images of the surface of MAC/MMT nanocomposite films in the dashed box area. As the MMT concentration increases, excessive agglomeration of MMT is observed on the surface of the MAC films.

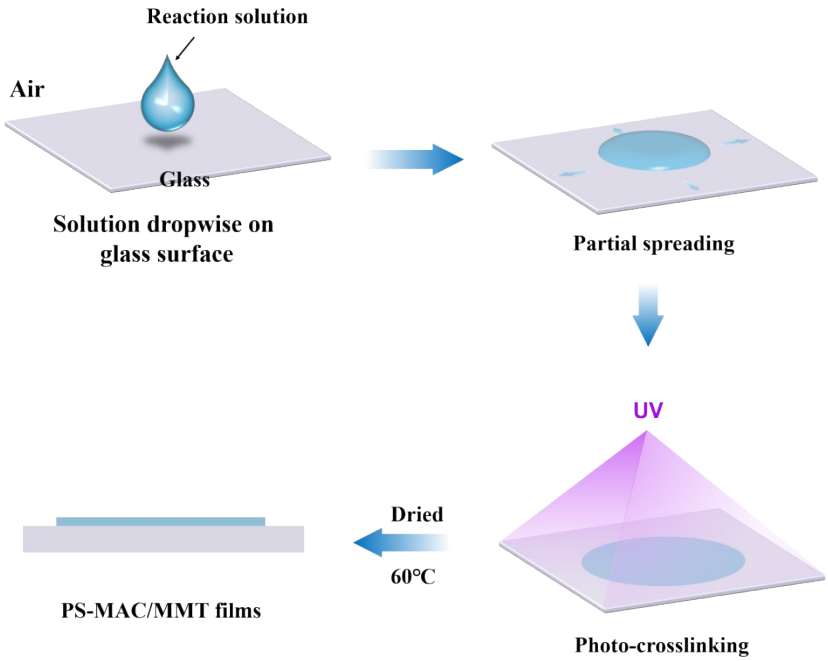

Figure S8. Schematic of the preparation of PS-MAC/MMT nanocomposite films with randomly assembled nanosheets via partial spreading on glass surfaces in air. The glass was not treated by plasma before using.

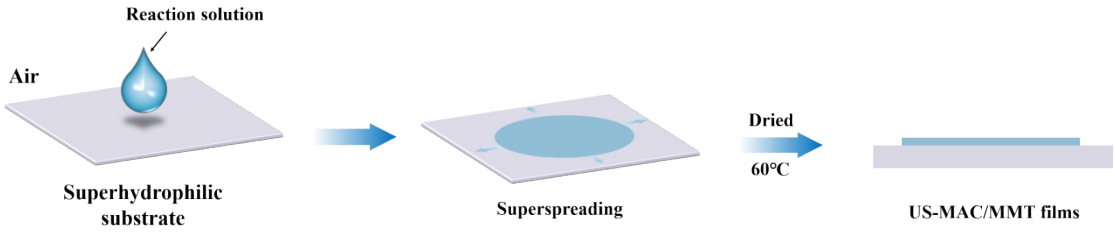

Figure S9. Schematic of the preparation of US-MAC/MMT nanocomposite films without UV photo-crosslinking. The glass was treated by plasma before using.

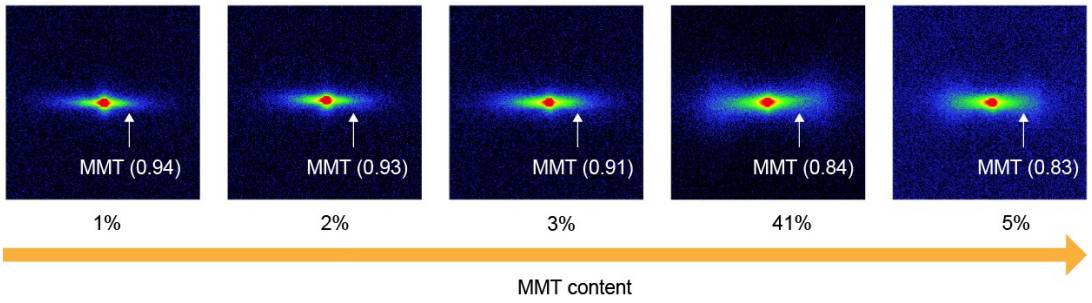

Figure S10. 2D SAXS images of MAC/MMT nanocomposite films with different MMT contents. With the increase of MMT content, the peaks in the SAXS pattern of MAC/MMT nanocomposite films gradually widen, but the nanosheets in these nanocomposite films are still highly aligned, as shown in Table S7.

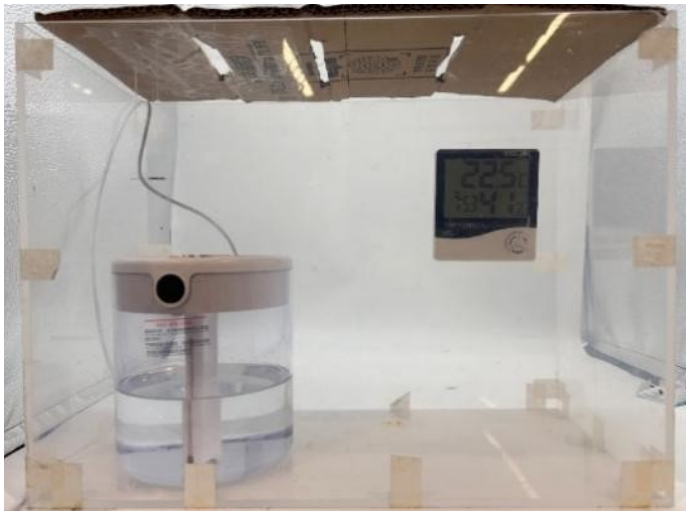

Figure S11. Device simulating a high relative humidity environment. Including humidifier, temperature and humidity device. Firstly, the environment in the transparent box was simulated to different humidities by a humidifier. After the humidity was stable, the sample was placed in the corresponding environment for 30 min. Finally, the mechanical properties of the sample were tested.

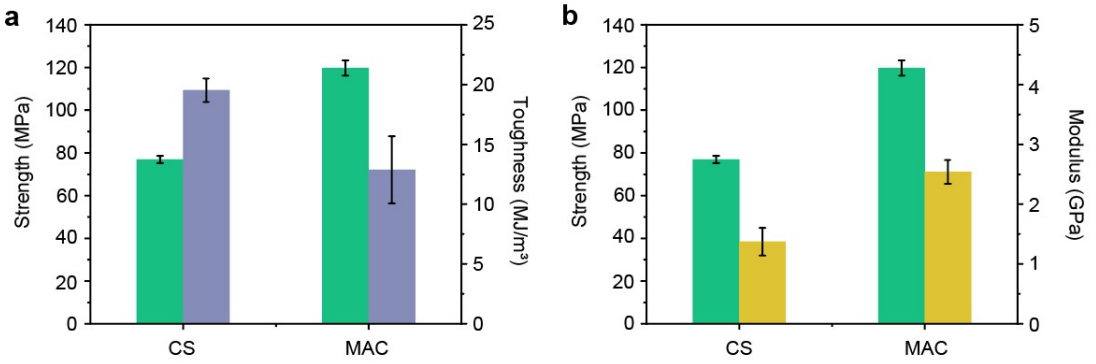

Figure S12. Mechanical properties of the CS and MAC films in 40% relative humidity environment. (a) The strength and toughness. (b) The strength and modulus. The composition of reaction solutions and the detailed mechanical properties data are listed in Table S9.

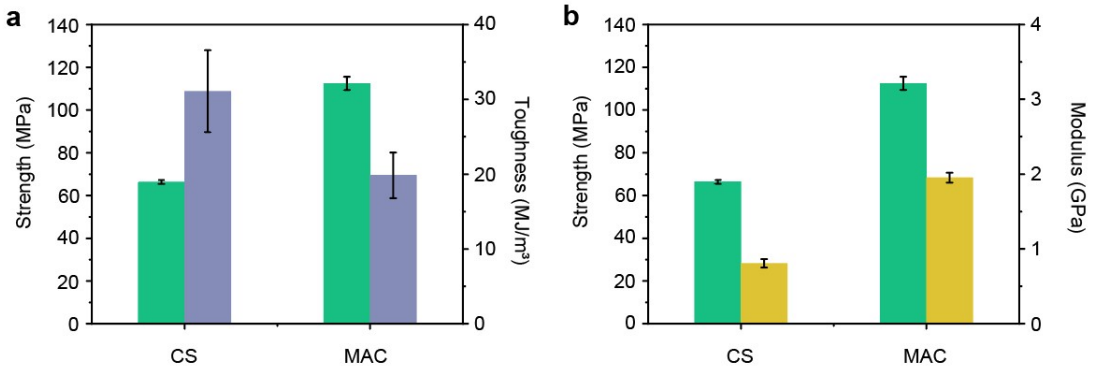

Figure S13. Mechanical properties of the CS and MAC films in 80% relative humidity environment. (a) The strength and toughness. (b) The strength and modulus. The composition of reaction solutions and the detailed mechanical properties data are listed in Table S11.

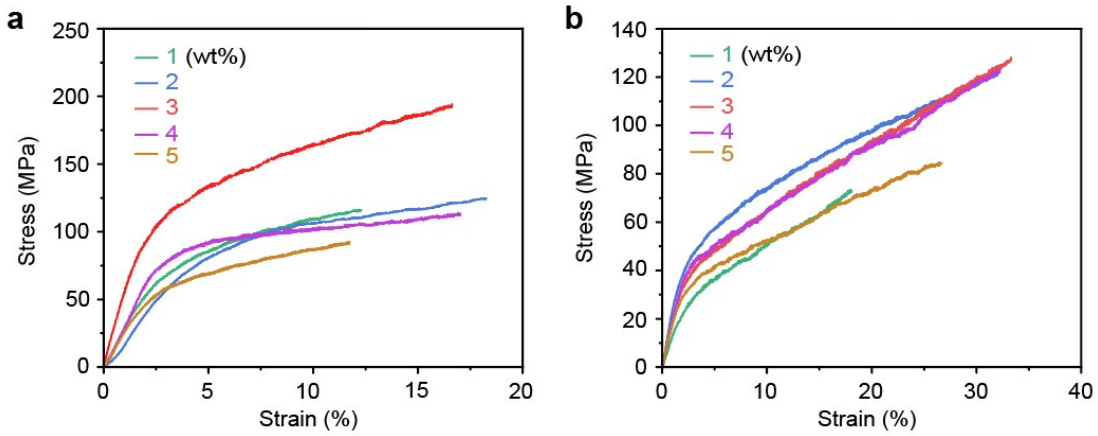

Figure S14. Tensile stress-strain curves of the MAC/MMT nanocomposite films in the environment of relative humidity of 40% and 80%. (a) Relative humidity of 40%. (b) Relative humidity of 80%. The composition of reaction solutions and the detailed mechanical properties data are listed in Table S10, 12.

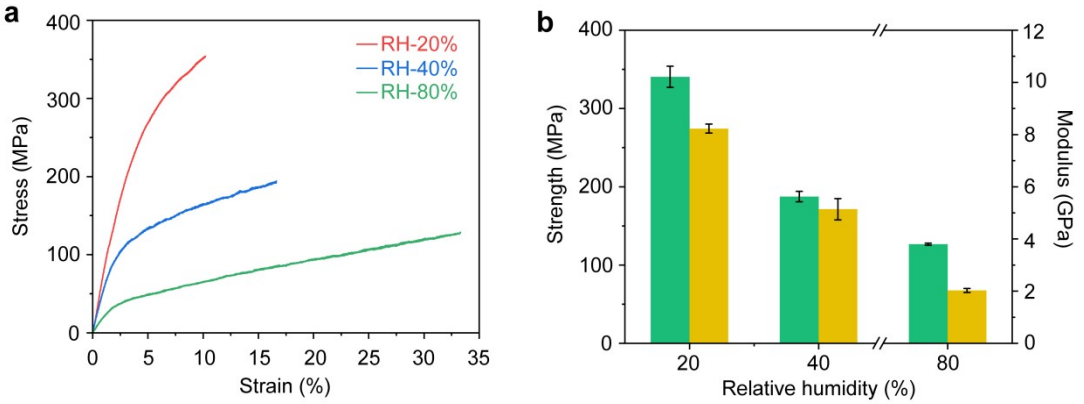

Figure S15. Mechanical properties of the MAC/MMT nanocomposite films in the different relative humidity environments. (a) Tensile stress-strain curves. (b) The strength and modulus. The composition of reaction solutions and the detailed mechanical properties data are listed in Table S3、10、12.

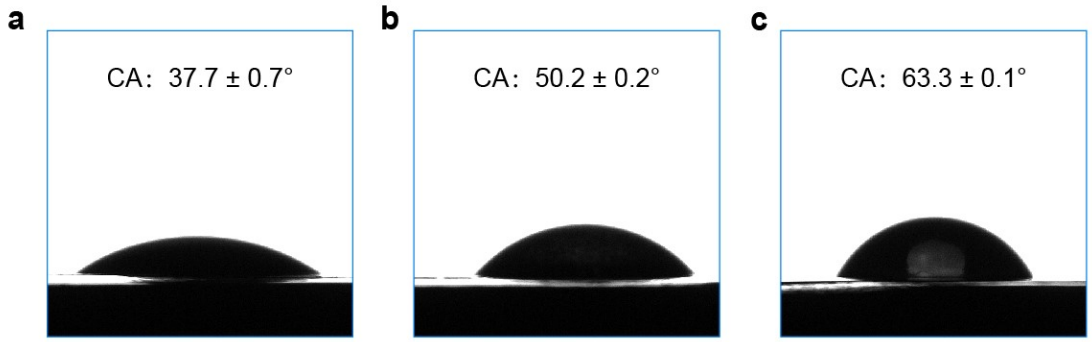

Figure S16. Water-droplet contact angle of the CS, MAC and MAC/MMT films in the air. (a) Photograph of a liquid droplet on CS films, showing strong hydrophilicity. (b) Photograph of a liquid droplet on MAC films. This MAC film with amidation leads to the reduction of free amino groups, which reduces the ability of CS to form hydrogen bonds with water molecules, thus reducing the hydrophilicity of the film. (c) Photograph of a liquid droplet on MAC/MMT films. The MMT dispersed within the crosslinked chitosan network can restrict the mobility of chitosan chains through hydrogen interactions, which further reduces its hydrophilicity.

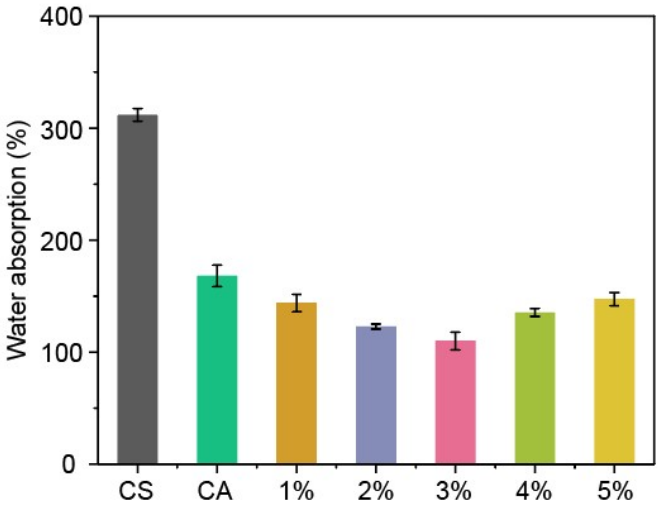

Figure S17. Analysis of water absorption performance. The water absorption of MAC/MMT-3% nanocomposite film is 109%, which is 202% lower than that of pure CS film.

Table S1. Summary of mechanical properties of MAC films with different concentrations. The data shown are mean ± standard deviation.

MAC / wt%	Strength / MPa	Strain / %
0.60	109.2 ± 1.2	22.1 ± 2.3
0.75	173.4 ± 10.2	14.4 ± 1.5
1.00	106.5 ± 3.4	19.1 ± 0.8
1.25	103.0 ± 1.1	20.8 ± 2.8
1.50	94.7 ± 0.2	16.8 ± 1.5

Table S2. Summary of mechanical properties of the CS and MAC films at 25℃ and 20% relative humidity. The data shown are mean ± standard deviation.

Film	Strength / MPa	Strain / %	Toughness / MJ/m^3	Modulus / GPa
CS	80.6 ± 0.3	23.3 ± 1.6	13.9 ± 0.4	1.7 ± 0.1
MAC	173.4 ±10.2	14.5 ± 1.6	17.3 ± 1.1	3.4 ± 0.1

Table S3. Summary of mechanical properties of MAC/MMT nanocomposite films with different MMT contents at 25℃ and 20% relative humidity. The data shown are mean ± standard deviation.

MMT / wt%	Strength / MPa	Strain / %	Toughness / MJ/m^3	Modulus / GPa
0	173.4 ± 10.2	14.5 ± 1.6	17.3 ± 1.1	3.4 ± 0.1
1	177.2 ± 3.9	9.9 ± 0.1	12.3 ± 0.1	4.3 ± 0.1
2	201.0 ± 8.1	10.2 ± 0.6	13.3 ± 1.5	4.5 ± 0.1
3	340.6 ± 13.4	9.2 ± 1.0	22.0 ± 2.5	8.2 ± 0.2
4	217.2 ± 4.7	10.4 ± 0.1	16.5 ± 0.4	6.5 ± 0.5
5	195.9 ± 0.5	10.8 ± 0.3	15.2 ± 1.2	4.5 ± 0.4

Table S4. Summary of mechanical properties of nanocomposite films obtained by superspreading strategy and partial spreading strategy. The data shown are mean ± standard deviation.

Film	Strength / MPa	Strain / %	Toughness / MJ/m^3	Modulus / GPa
CS	80.6 ± 0.3	23.3 ± 1.6	13.9 ± 0.4	1.7 ± 0.1
MAC	173.4 ± 10.2	14.5 ± 1.6	17.3 ± 1.1	3.4 ± 0.1
PS-MAC/MMT	191.8 ± 16.8	21.7 ± 0.8	29.4 ± 3.0	4.1 ± 0.2
US-MAC/MMT	207.8 ± 2.6	21.2 ± 1.8	30.6 ± 2.5	4.6 ± 0.3
MAC/MMT	340.6 ± 13.4	9.2 ± 1.0	22.0 ± 2.5	8.2 ± 0.2

Table S5. Summary of mechanical properties of the chitosan nanocomposite films in other literatures and this work.

Nanonanocomposite films	**Strength / MPa**	**Toughness / MJ/m^3**	**Modulus / GPa**	**Ref.**
MMT-CS	103.0	—	6.8	2
CS/PVA-MtC	143.4	—	0.1	3
Zn^{2+}-GO-CS	220.0	2.5	5.4	4
TiO_2-CS	16.8	—	0.5	5
SiO_2-CS	30.0	9.0	1.2	6
MXene-CS	50.9	—	4.4	7
LNS-CS	27.5	—	0.5	8
CNFs-CS	127.8	—	5.8	9
CNC-CS	75.0	—	0.7	10
CNW-CS	24.4	—	0.8	11
Chitin-CS	110	—	1.7	12
This work	340.6	22.0	8.2	—

Table S6. Summary of the thermal decomposition temperature of CS，MAC and MAC/MMT films.

Film	Temperature / ℃
CS	238.3
MAC	255.5
MAC/MMT	286.8

Table S7. Summary of the *f* values of 2D SAXS of MAC/MMT nanocomposite films with different MMT contents.

MMT / wt%	***f***
1	0.94
2	0.93
3	0.91
4	0.84
5	0.83

Table S8. Summary of the light transmittance of CS, MAC, MAC/MMT and PS-MAC/MMT films.

Film	Transmittance / %
CS	94.1
MAC	81.3
MAC/MMT	80.6
PS-MAC/MMT	45.1

Table S9. Summary of mechanical properties of the CS and MAC films in 40% relative humidity environment. The data shown are mean ± standard deviation.

Film	Strength / MPa	Strain / %	Toughness / MJ/m^3	Modulus / GPa
CS	76.9 ± 1.6	34.9 ± 1.5	19.5 ± 0.9	1.3 ± 0.2
MAC	119.7 ± 3.5	14.6 ± 2.6	12.8 ± 2.8	2.5 ± 0.2

Table S10. Summary of mechanical properties of MAC/MMT nanocomposite films with different MMT contents in 40% relative humidity environment. The data shown are mean ± standard deviation.

MMT / wt%	Strength / MPa	Strain / %	Toughness / MJ/m^3	Modulus / GPa
0	119.7 ± 3.5	14.6 ± 2.6	12.8 ± 2.8	2.5 ± 0.2
1	112.8 ± 2.9	11.7 ± 1.1	8.8 ± 1.4	2.4 ± 0.2
2	122.6 ± 2.1	16.7 ± 1.6	14.9 ± 1.6	2.5 ± 0.1
3	187.5 ± 6.6	15.3 ± 1.3	21.1 ± 2.8	5.2 ± 0.4
4	107.2 ± 6.1	18.8 ± 1.8	15.7 ± 0.3	2.8 ± 0.1
5	93.4 ± 1.0	11.5 ± 0.2	7.8 ± 0.1	2.5 ± 0.1

Table S11. Summary of mechanical properties of the CS and MAC films in 80% relative humidity environment. The data shown are mean ± standard deviation.

Film	Strength / MPa	Strain / %	Toughness / MJ/m^3	Modulus / GPa
CS	66.3 ± 0.9	67.8 ± 12.7	31.1 ± 5.5	0.8 ± 0.1
MAC	112.4 ± 3.1	27.8 ± 5.8	19.8 ± 3.0	2.0 ± 0.1

Table S12. Summary of mechanical properties of MAC/MMT nanocomposite films with different MMT contents in 80% relative humidity environment. The data shown are mean ± standard deviation.

MMT / wt%	Strength / MPa	Strain / %	Toughness / MJ/m^3	Modulus / GPa
0	112.4 ± 3.1	27.8 ± 5.8	19.8 ± 3.0	1.9 ± 0.1
1	71.0 ± 1.9	12.2 ± 5.9	5.6 ± 2.7	1.3 ± 0.3
2	115.5 ± 6.2	34.6 ± 2.6	25.6 ± 1.4	1.7 ± 0.3
3	126.6 ± 1.4	29.3 ± 3.9	26.6 ± 0.4	2.0 ± 0.1
4	118.3 ± 4.8	23.6 ± 8.6	18.8 ± 6.6	1.9 ± 0.1
5	81.8 ± 2.6	20.6 ± 6.0	11.5 ± 3.8	1.7 ± 0.3

Reference

1. W. Chen, P. Zhang, R. Zang, J. Fan, S. Wang, B. Wang and J. Meng, *Adv. Mater.*, 2020, **32**, 1907413.
2. H. Yao, Z. Tan, H. Fang and S Yu, *Angew. Chem. Int. Ed.*, 2010, **52**, 10127-10131.
3. K. El. Bourakadi, N. Merghoub, M. Fardioui, M. E. M. Mekhzoum, I. M. Kadmiri and E. M. Essassi, *Compos. Part B Eng.*, 2019, **172**, 103-110.
4. S. Liu, F. Yao, O. Oderinde, K. Li, H. Wang, Z. Zhang and G. Fu, *Chem. Eng. J.,* 2017, **321**, 502-509.
5. J. Vallejo-Montesinos, J. Gámez-Cordero and R. Zarraga, *Polym. Bull.*, 2020, **77**, 107-133.
6. W. Zhang, W. Zhou, Z. Zhang, D. Zhang, Z. Guo, P. Ren and F. Liu, *Polymers*, 2023, **15**, 4015.
7. Y. Wang, B. Jiang and T. Sun, *J. Mater. Chem. C*, 2022, **10**, 8043-8049.
8. M. Madadi, M. Elsayed, G. Song, R. Kumar, M. Mahmoud-Aly, B. Basak, B.H. Jeon and F. Sun, *Chem. Eng. J.*, 2023, **465**, 14288.
9. P. Falamarzpour, T. Behzad and A. Zamani, *Int. J. Mol. Sci.*, 2017, **18**, 396.
10. H. Mao, C. Wei, Y. Gong, S. Wang and W. Ding, *Polymers*, 2019, **11**, 166.
11. S. Y. Rong, N. M. Mubarak and F. A. Tanjung, *J. Environ. Chem. Eng.*, 2017, **5**, 6132-6136.
12. B. Ma, A. Qin, X. Li, X. Zhao and C. He, *Int. J. Biol. Macromol.*, 2014, **64**, 341-346.